Authors' accepted manuscript
Article published in *Resources, Conservation and Recycling*, Volume 170, July 2021, 105584
https://doi.org/10.1016/j.resconrec.2021.105584

Evaluation of the reactivity of treated spent pot lining from primary aluminum production as cementitious materials

Victor Brial[1], Hang Tran[2], Luca Sorelli[2], David Conciatori[2], Claudiane M. Ouellet-Plamondon[1*]

Abstract

Aluminum Spent Pot lining (SPL) is an industrial hazardous waste generated from aluminum electrolysis cells. The SPL separates in two parts, the first cut is rich in carbonaceous materials and the second cut is rich in vitrified refractory. Treating second cut SPL by the Low Caustic Leaching and Liming (LCL&L) process generates an inert non-hazardous residue, called LCLL Ash. This product is mainly composed of stable crystalline phases such as corundum, albite, nepheline with some amount graphite. Ground as a fine powder, LCLL Ash could be used in cement as a supplementary cementitious material (SCM). This paper focuses on the investigation of LCLL Ash reactivity and its improvement by calcination at 1050°C. Reactivity was evaluated with multiple tests, such as compressive strength activity index, Frattini test and Rilem R^3 tests followed by XRD analysis. An inert SCMs (limestone, filler, and quartz) and reactive SCMs (slag, fly ash, silica fume) were used as references. The results show that LCLL Ash in cement shows inert properties similar to quartz with a retarder effect below 7 days and a high alkali content. Moreover, the temperature of the Rilem R^3 tests, shows expansion in the paste due to LCLL Ash hydro reactivity. This expansion was not observed with LCLL Ash blended cement mortar. Calcination improved significantly the reactivity of LCLL Ash by generating higher reactive silica and alumina content. Notably, calcined LCLL Ash showed reaction properties similar to a calcined clay. Finally, neither delay on hydration nor expansion was observed with calcined LCLL Ash.

Keywords: Low Caustic Leaching Liming, Treated Spent Pot Lining, Blended cement, Hazardous Waste, Aluminum, Supplementary Cementitious Materials

[1] Department of Construction Engineering, École de Technologie Supérieure, Canada
[2] Department of Civil and Water Engineering, Université Laval, Canada

*Corresponding author:*claudiane.ouellet-plamondon@etsmtl.ca;*

École de technologie supérieure

1100, rue Notre-Dame Ouest

Montréal (Québec) Canada H3C 1K3

1. Introduction

With a production of 4 billion tons in 2018, concrete is one of the most consumed materials in the world (Andrew, 2019). However, the concrete industry is a major consumer of natural resources and energy causing major greenhouse gas emissions (GHG). In particular, the production of one ton of Portland clinkers can produce up to 1 ton of CO_2 of which 60% of comes from unavoidable decarbonation reactions (Strazza, Borghi Del, Gallo and Del Borghi, 2011). Such emissions have a major impact and represent every years 5-8% of global CO_2 emissions (Le Quéré et al., 2015; Lehne and Preston, 2018). Various solutions are implemented to reduce GHG of cement industry. Optimizing manufacturing processes to make them more energy efficient and using supplementary cementitious materials (SCM) are ways to reach this goal (Kajaste and Hurme, 2016; Shanks et al., 2019; WBCSD and IEA, 2009). The partial replacement of cement with SCMs in concrete applications provide advantages from an economic and ecological point of view (Aïtcin and Flatt, 2015; Hewlett et al., 2004; Tokyay, 2016). These benefits pushed different industries to add supplementary treatments to optimize waste revalorization in cement (Zhang et al., 2013). Therefore, SCMs partially replace cement and are generally industrial by-products or wastes such as fly ash, silica fumes or blast furnace slags. SCM can be divided in three categories: latent hydraulic, pozzolans or inert materials (Hewlett et al., 2004; Tokyay, 2016). Besides the benefits on the carbon footprint of concrete, SCM allows a better valorization of non-conventional waste and reducing landfill (Agrawal et al., 2004).

For instance, the primary aluminum industry produces industrial wastes, such a spent pot lining (SPL) from electrolysis cells. Every ton of aluminum generated about 22 kg of SPL (Birry et al., 2016),which represents approximately 70,000 tons of SPL generated every year in Canada. SPL is a hazardous substance due to its leachable content in fluoride and cyanide, but also due to its hydro reactivity creating explosive gases (Kimmerle et al., 1993; Øye, 2017). SPL can be separated in two parts: the first cut is rich in carbonaceous materials coming from the cathode and the second cut consists in vitrified refractory. Developed in the 1990's, the LCL&L (Low Caustic Leaching & Liming) process, through hydro metallurgic way, transforms SPL into an inert material. The second cut of SPL, when treated by LCL&L process, turns into an inert material called LCLL Ash (named ''LCLL'' in this paper) studied in this article (Birry et al., 2016). LCLL ash is a grey

powder, mainly composed of oxides of silicon and aluminum, with minor fractions of calcium, iron, sodium, and fluor oxides. This composition is comparable to a clay.

A similar by-product developed by a pyro metallurgic treatment of SPL allowed to obtain glass frit (GF) (Fares, 2008). This by-product was tested as a cementitious binder for incorporation into binary, ternary and quarterly mixtures. However, GF was studied for alkaline activation. The results demonstrate that GF has a similar reactivity to a latent hydraulic binder with a behavior similar to slag (Fares, 2008; Laldji and Tagnit-Hamou, 2016). The binary GF mixture exhibited slightly lower compressive strengths than the unblended mixture at early age of hydration, but greater compressive strength after 28 days. In addition, the GF exhibited a remarkable durability against freezing-thawing (resistance similar to the unblended mixture), lower chloride ion permeability, and improved resistance to the alkali silica reaction (Laldji and Tagnit-Hamou, 2016; Nova Pb inc., 2004).

In 2018, 2.47 million tons of primary aluminum were produced only in Quebec (Natural Resources Canada, 2019). The production of primary aluminum by the Hall-Heroult process generates hazardous wastes, then treated but currently unpreventable. The major advantage of SPL revalorization for this industry is to decrease the environmental impact of primary aluminum by avoiding the SPL landfilling. Using SPL without pretreatment in cement plants as a raw material is a common practice in Europe, Asia, Australia, Brazil and the Middle East (Broek and Øye, 2018; Jawi et al., 2020; Nunez, 2020; Personnet, 1999). For example, EGA in the United Arab Emirates promotes the use of SPL without hydro or pyro pretreatment, enforcing crushing and sieving. Thanks to the fluoride content, the addition of SPL in the raw meal decreases the clinkerisation temperature by 20°C to 100°C according to the SPL replacement percentage (Gomes et al., 2005; Jawi et al., 2020). This allows to reduce the fossil fuels consumption up to 4% and reduce the overall CO_2 emissions by 1%. However, the high sodium content limits the use of SPL in cement plants from 0.2% to 0.75% to avoid durability concerns in concrete due to the alkalis silica reactions (Broek and Øye, 2018; Gomes et al., 2005; Jawi et al., 2020; Nunez, 2020). In North America, this practice in raw cement meal is not allowed due to the high percentage of fluoride in SPL.

For the concrete and construction industry, replacing a part of cement by treated SPL, can decrease the carbon footprint of concrete. The reuse of this local waste in Quebec can provide a new source of supplementary cementitious materials (SCM) and would limit the conventional SCM import from USA or Europe, such as fly ash or slag. This could further diminish the carbon footprint of concrete by limiting the transportation of conventional SCMs. The project aims to demonstrate the potentials of a circular economy, where the waste from one industry can feed in the other.

The purpose of this article is to study and understand the reactivity of the LCLL Ash in cement to avoid its landfilling. Moreover, the improvement of LCLL Ash reactivity was studied with an additional high temperature calcination treatment to increase the amorphous content. Hence, this article aims to answer the following questions:

(i.) Is the LCLL Ash reactive? What is its type of reactivity?

(ii.) Is it possible to increase the reactivity of LCLL Ash by calcination?

To answer these questions, this study evaluates the reactivity of LCLL Ash as well as calcined LCLL Ash according to three reactivity tests. Calcination is a common method to turn some mineral materials, such as clay or shale, into reactive SCMs (Ambroise et al., 1985; Mather, 1958; Murat, 1983). Replacing until 20 % of clinker in cement by calcined materials, allows to reach similar or better properties than unblended Portland cement (Li et al., 2015; Trümer and Ludwig, 2015). Currently, the most studied calcined materials are calcined clays, particularly clays with a high kaolinite content. A good example of calcined clay use is Limestone Calcined Clay Cement (LC3) which allows to make cementitious materials by replacing 50% of clinker with a mix of calcined clay and limestone (Cancio Díaz et al., 2017; Dhandapani et al., 2018; Favier and Scrivener, 2018; Scrivener et al., 2018). LC3s show similar or better properties than unblended Portland cements, particularly mechanical and durability properties (Dhandapani et al., 2018; Scrivener et al., 2018). Calcinating mineral materials to replace cement can seem counterintuitive, however, blended cement with calcined clay or calcined shale have a lower carbon footprint than unblended cement. This advantage stems from the uncalcined calcite and a lower calcination temperature of clay than clinker (Miller et al., 2018; Scrivener et al., 2018). Since LCLL Ash has a similar composition to clay, we can expect calcination to improve its reactivity in cement. For each test, LCLL Ash and calcined LCLL Ash was compared to others inert and reactive materials

such as quartz powder, limestone filler and slag, fly ash, silica fume respectively. In the first analysis of mortar compressive strength, these materials were individually blended with cement to evaluate the mixes' relative strength activity index. This observation was followed by Frattini tests to evaluate the pozzolanic activity of each material. To confirm the previous observations, the Rilem R^3 tests (Li et al., 2018) were conducted to study the materials' reactivity without the interference of cement. Quantitative X-ray diffraction tests followed to deepen the understanding of the reactivity of LCLL Ash and calcined LCLL Ash. The effect of the different SCMs replacement on the fresh properties was evaluated by measuring the yield stress and the plastic viscosity. Finally, the effect of SCMs on the microstructure was analyzed with mercury intrusion porosimetry (MIP) and scanning electron microscopy images (SEM).

2. Materials and methods

2.1.Materials

In this study, the LCLL Ash comes from the Rio Tinto treatment plant based in Jonquière, QC, Canada. For the rest of the paper, LCLL will refer to LCLL Ash. A plain Portland cement (Type GU, Ciment Québec, QC, Canada) was used to prepare mortar and Frattini tests. The LCLL reactivity was compared to two fly ashes: FA-E (Type F fly ash, Ciment Québec, QC, Canada), and FA-PA (Type F fly ash, ProAsh, VA, USA). LCLL was also compared to a slag GGBS (Type S ground granulated blast furnace slag, Lafarge, ON, Canada) and a blue silica fume (Silicium Québec, QC, Canada). Moreover, two inert materials were used, a limestone filler (Pulverized limestone, Graymont, QC, Canada) and a quartz powder made by grounding graded Ottawa sand, respectively named FC and Q.

Table 1: Chemical composition of cement and SCMs.

Oxide	Percentage in weight (wt%)								
	OPC	**FC**	**SF**	**LCLL**	**Calcined LCLL**	**Q**	**FA-E**	**FA-PA**	**GGBS**
SiO_2	19.2	2.2	96.5	37.2	38.8	91.	58.5	58.5	38.6
Al_2O_3	4.7	0.4	0.5	36.3	36.6	4.9	19.6	20.9	10.3
Fe_2O_3	3.61	0.14	0.45	7.36	8.59	1.72	5.89	7.23	2.13
CaO	61.5	53.6	0.4	3.0	4.0	0.6	5.5	3.6	35.7
MgO	2.4	0.5	0.4	0.4	0.4	0.0	2.0	2.0	8.8
SO_3	3.98	0.10	0.08	0.06	0.12	0.00	0.21	0.14	2.08
K_2O	1.06	0.13	0.66	0.77	0.79	0.10	1.91	2.35	0.78
Na_2O	0.25	0.02	0.11	8.23	8.03	1.09	1.03	1.10	0.43
TiO_2	0.25	0.01	0.00	0.75	0.78	0.10	0.82	0.90	0.56
P_2O_5	0.14	0.01	0.10	0.12	0.10	0.01	0.58	0.21	0.04
V_2O_5	0.01	0.00	0.00	0.03	0.03	0.01	0.04	0.69	0.11
LOI at 1000° C	2.6	42.9	0.6	5.7	1.1	0.0	3.6	2.9	0.1

The chemical composition of cement used for the blended mixes and SCM samples, both in anhydrous conditions, was measured by X-ray fluorescence (XRF) bed fusion. Chemical and SCMs compositions are shown in Table 1 and on ternary diagram on Fig 1b. The composition of LCLL is closer to a calcined clay composition, both showing a high silica and alumina content. However, LCLL shows a high alkali content with about 8% in weight of sodium oxide. The mineralogical compositions of the materials were obtained by X-ray powder diffraction (XRD) with Rietveld analysis. For SCMs, the external standard method was used to determine the amorphous content. The mineralogical composition of the cement for the blended mixes and SCM samples, anhydrous, were measured by quantitative XRD (Table 2).

Table 2: Major mineralogical compositions of OPC and SCM. (: Aluminium oxide silicate, **: Calcium magnesium aluminum silicon oxide)*

Phase	OPC	FC	SF	LCLL	Calcined LCLL	Q	FA-E	FA-PA	GGBS
C_3S	**63.4**	-	-	-	-	-	-	-	-
C_2S	**7.3**	-	-	-	-	-	-	-	-
C_3A	**3.9**	-	-	-	-	-	-	-	-
C_4AF	**13.0**	-	-	-	-	-	-	-	-
Quartz	**0.1**	**0.3**	**0.3**	**6.7**	**2.4**	**98.5**	**5.5**	**10.0**	-
Corundum	-	-	-	**14.5**	**8.4**	-	-	-	-
Albite	-	-	-	**20.2**	**0.9**	-	-	-	-
Nepheline	-	-	-	**18.7**	**3**	-	-	-	-
Anorthite	-	-	-	**11.8**	**5.4**	**1.1**	-	-	-
Graphite	-	-	-	**6.9**	**3.6**	-	-	-	-
Mullite	-	-	-	**3.8**	-	-	-	**0.3**	-
Hematite	-	-	-	**2.6**	-	-	**0.4**	**0.3**	-
Magnetite	-	-	-	**4.2**	-	-	-	-	-
Calcite	**2.2**	**97.2**	-	-	-	-	-	-	-
Dolomite	-	**2.5**	-	-	-	-	-	-	-
AS*	-	-	-	-	-	-	**6.1**	**3.3**	-
CMAS**	-	-	-	-	-	-	-	-	**6.8**
Amorphous	-	-	**98.9**	**5.9**	**74.9**	-	**87.9**	**86.2**	**93.1**

The LCLL is composed of crystalline materials such as corundum, albite, nepheline, quartz and anorthite with low content of amorphous. An additional treatment by calcination was realized to validate its impact on LCLL reactivity. To achieve this treatment, LCLL was calcined at 1050°C in a muffle furnace for 30 minutes followed by a rapid air cooling at room temperature. Calcination temperature was selected according to a previous study on synthetic ashes with a comparable composition (Wang et al., 2017). The calcination of LCLL did not affect its chemical composition but it decreased the loss of ignition from 1% to 5%. However, in this case, the calcination changes considerably LCLL's phase composition by decreasing albite, nepheline, quartz and anorthite content. Calcination greatly increases the amorphous, content from 6% to 75%.

For each material studied, the particle size distribution (PSD) was measured using Malvern Mastersizer\E by laser diffraction granulometry with isopropanol as dispersant. The particle sizes distributions are presented in Fig. 1b. Each material was ground with a planetary grinder to reach a d_{50} around 10 to 20 µm. Due to its particle size, silica fume was not ground.

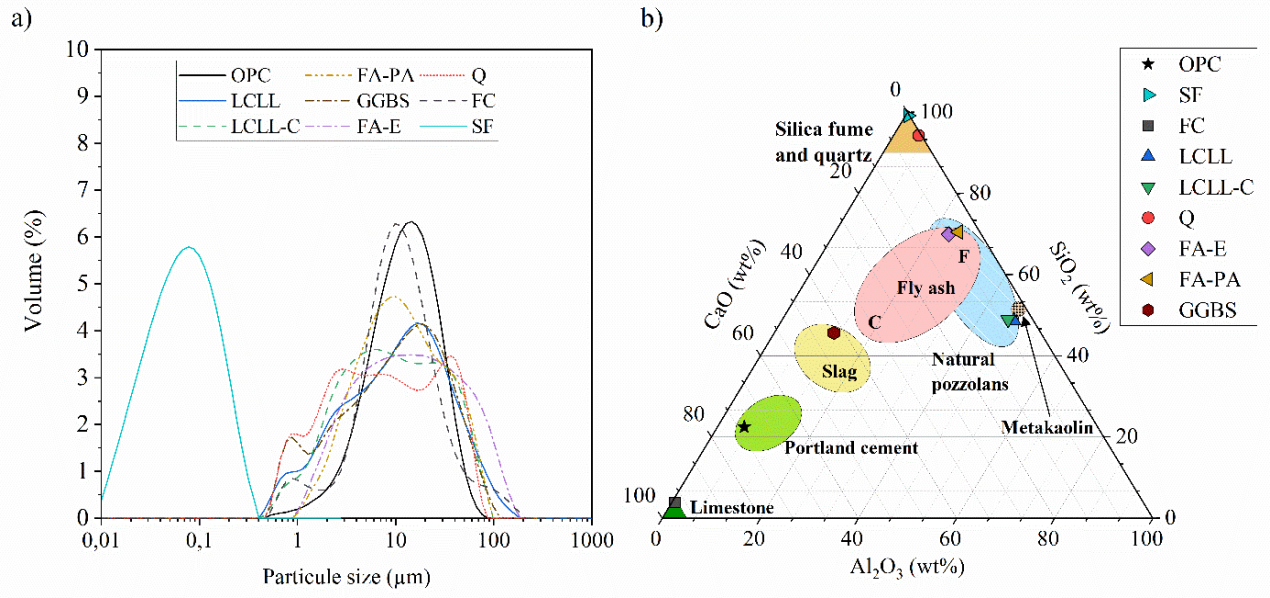

Figure 1: a) Particle size analysis by laser granulometry b) CaO-SiO_2-Al_2O_3 ternary diagram of cement and SCMs.

2.2. Methods

2.2.1. Mortar

The target replacement level of cement by SCMs was set at 20% in weight as adequate to observe the contribution of SCMs in cement. The value was chosen according to (Donatello et al., 2010), and to remain consistent with Frattini tests. The procedure used was based on ASTM C109-16a (ASTM International, 2016). Control mortar cubes were prepared by mixing 2915 g graded Ottawa sand, 1060 g GU type cement and 514 mL water according to the ASTM C305-14 (ASTM International, 2015). For each mix, the Portland cement and SCM were dry mixed inside a micro-Deval apparatus for 15 minutes with 1500 g of charge (steel balls) to ensure homogeneous mixing. To avoid differences on the particles size, each sample was prepared in the same manner including the 100% cement reference. The different mixes were tested at 1, 7, 28 and 112 days to evaluate the strength activity index through time. To keep a constant water/binder ratio of 0.485 and a constant flow of 110 ± 5 (ASTM International, 2010), about 5 to 15 mL of polycarboxylate super plasticizers was used.

185 2.2.2. Frattini

186 The Frattini test evaluates portlandite saturation in a supernatant solution of a hydrated Portland
187 cement and a pozzolanic test material by measuring the [OH^-] and [Ca^{2+}] concentrations
188 (Donatello et al., 2010; Tironi et al., 2013). The preparation process requires to create a mix of 16
189 g of Portland cement and 4 g of SCM with 100 mL of distilled water. Samples were then left for 8
190 days, in a sealed plastic bottle, in an oven at 40°C. After 8 days, samples were filtered through a
191 0.2 µm syringe filter. In this study the HO^- concentration was measured by titration against dilute
192 HCl with methyl orange indicators. Calcium concentration was measured by ICP-OES Agilent
193 5110 at 317.9 nm from a 1000 ppm calcium standard. The test was carried out to evaluate the
194 pozzolanic reactivity. However, this test is not sufficient to compare inert or hydraulic reactivities.
195

196 2.2.3. R^3: Heat release, CH consumption

197 Initially, this model was developed by a Rilem technical group to study the reactivity of calcined
198 clay and its use was extended to other SCMs (Avet et al., 2016). Nowadays, the R^3 model is non-
199 standardized method used to evaluate the reactivity of SCMs in a paste composed of 33.33 g of
200 portlandite ($Ca(OH)_2$), 11.11 g of SCM, and 5.56 g calcite ($CaCO_3$) in a solution of 60 mL of
201 deionized water with 0.24 g of KSO_4 and 1.20 g KOH (Li et al., 2018). Such chemical composition
202 has the advantage to recreate the chemical behavior of limestone cement, without cement particles.
203 This allowed to study the reactivity of SCMs alone, without chemical activity of cement particles.
204 For this study, the R^3 system measurement focuses on heat released at 7 days measure by
205 isothermal calorimetry and portlandite consumption. These two tests were selected to show the
206 calcium hydroxide consumption versus heat released and determine the type of reactivity of tested
207 materials according to the method proposed by (Suraneni et al., 2019). Isothermal calorimetry at
208 40°C was carried out to measure the heat release of the R^3 systems for 7 days. For each calorimetry
209 test, initial and final baselines were recorded for 180 minutes. The portlandite consumption was
210 measured by TGA analyses. Samples were retrieved from the R^3 calorimetry ampoules were
211 carefully rolled in adhesive tape to minimize glass contamination and were broken to collect the
212 paste inside. The hydration of the samples was stopped by solvent exchange as described by
213 (Scrivener et al., 2016; Snellings et al., 2018). For each test, 50 mg of anhydrous sample was
214 introduced in the crucible. The weight loss was recorded from 30 to 950°C with a heating rate of
215 10°C/min in a protective nitrogen atmosphere at a flow rate of 50 mL/min. The portlandite weight

loss was determined by using the tangent method described by (Scrivener et al., 2016) and the portlandite consumption was calculated as g/ 100 g SCM according to Eq.1 (Li et al., 2018).

$$m_{CH,consumption} = 100 \times \frac{(m_{0,CH,ignited} - m_{CH,ignited})}{m_{0,SCM,ignited}} \quad \text{Eq. (1)}$$

where $m_{0,CH,ignited}$ and $m_{0,SCM,ignited}$ are respectively the initial portlandite content and SCM content in the R^3 mix on the ignited basis. The residual CH ($m_{CH,ignited}$) (g/ 100 g ignited base) in the R^3 mixes was calculated according to Eq.2:

$$m_{CH,ignited} = 100 \times \frac{\Delta m_{H_2O,CH} \times 74.09}{18.02 \times m_{950}} \quad \text{Eq. (2)}$$

where $\Delta m_{H_2O,CH}$ is the weight loss of the sample for portlandite using the tangent method, and m_{950} is the weight of the sample at 950°C.

2.2.4. X-ray diffraction

The R^3 mixes were analyzed by XRD to identify the minerals phases precipitated by the reaction of the tested materials in the R^3 paste. XRD data were collected using Cu K-alpha radiation on Bruker D8 Advance diffractometer operated at 40 kV 40 mA. Measurements were made with a flat-plate Bragg-Brentano geometry incident beam and receiving Soller slits of 0.04 rad were used. The incident beam divergence slit was fixed at 0.26° (0.5 mm). A beam knife was used to reduce air scattering and a receiving anti-scatter slit of 1.10° (2.5 mm) was positioned in the diffracted beam path. A Lynxeye 1D linear position-sensitive X- ray detector with a length of 2.951°2θ was used for data acquisition. During measurements, the samples were spun around the vertical goniometer axis at 15 rpm to improve particles statistics and measured over an angular range of 5 to 70°2θ with a 0.020°2θ step size. With an accumulated time per step of 0.50 s, total measurement time was of 28 min per scan. The amorphous content was measured by a ZnO external standard. The mass absorption coefficient was corrected by calculations from the XRF oxide composition, and the bound water content from the TGA measurement.

2.2.5. Mercury intrusion porosimetry

The influence of each tested material on the pore structure and the porosity were measured by mercury intrusion porosimetry (MIP). A cylindrical specimen of cement paste composed of 80 % cement and 20 % SCM in weight with a water/binder ratio of 0.485 were cured under water for 28

days. This samples were sawed under cutting oil using a wheel saw to obtain a 1.5 mm thick slide with a weight between 1 to 1.5 g.

The selection of the drying method is an important impact on MIP results (Gallé, 2001; Mindess et al., 2003; Moukwa and Aitcin, 1988; Scrivener et al., 2016). For example, Oven drying show increased the total volume percolated, freeze-drying and vacuum drying show a similar percolated volume with some change in the pore's distribution. In this study, the solvent exchange method was selected as method to dry the sample because it seems the most adapted technique (Ma, 2014; Scrivener et al., 2016). However, this technique is not entirely be representative of the porosity in an undried material.

The sample slides were broken in 4 parts and rinsed in isopropyl alcohol to remove the excess of cutting oil. The water in the pores were removed by immersing the samples in 150 mL of methanol for 7 days before a vacuum drying at 40°C. The MIP tests were performed with a Micromeritics Autopore IV 9500 which determines pore sizes in the range of 3 nm to 50 μm (corresponding to a 0.014 MPa–225 MPa range of applied pressure) in step mode with a contact angle of 130°. However, due to some limitation as the ink bottle effect, the pore model, and the restriction to the open porosity, the true pore structure cannot be described by MIP however, the technique is still valuable in making comparative assessments of the pore size changes (Abell et al., 1999; Diamond, 2000; Moro and Böhni, 2002; Scrivener et al., 2016).

2.2.6. Determination of rheological properties

The influence of tested materials on the rheological properties were studied on cement pastes composed of 64.0 g of cement, 16.0 g of SCMs and 38.8 g of distilled water. The mixing procedure was completed following the ASTM C1738, the paste obtain with this standard is expected to have rheological properties analogous to a concrete without its aggregates (ASTM International, 2014; Ferraris et al., 2001). The of rotational speed and torque were measured with the 3D printed geometry recommended by the NIST on the Anton Paar MCR 302 rheometer equipped with a CC27 cup and a C-PTD 200 temperature controller. The 3D geometry is a double spiral spindle with a diameter of 25 mm and is 55 mm long from the bottom to the top of the spiral. The geometry

was 3D printed in EOS StainlessSteel CX and was calibrated according to the NIST recommendations with the SRM 2493 (Ferraris et al., 2015; Olivas et al., 2017).

The cement pastes were tested 15 minutes after the contact water/cement. The test consists in an up-curve of 18 measurements from 0.1 rpm to 100 rpm and a down curve of 23 measurements from 100 rpm to 0.1 rpm. Each measurement is a step during 15 s until the stabilization of the torque. The shear stress τ, the shear rate $\dot{\gamma}$ and the apparent viscosity μ are calculated thanks to the following equations where N and Γ are respectively the rotational speed and the torque (Eq. 3, Eq. 4, Eq. 5). The parameters Kτ and Kμ are determined by the calibration of 3D printed geometry with the SRM 2493.

$$\tau = K\tau \times \Gamma \quad \text{Eq. (3)}$$

$$\dot{\gamma} = \frac{K\tau}{K\mu} \times N \quad \text{Eq. (4)}$$

$$\mu = K\mu \times \frac{\Gamma}{N} \quad \text{Eq. (5)}$$

By considering the Bingham model, the yield stress τ_0 and the plastic viscosity μ are respectively estimated as the y-intercept and the slope of the linear regression of the curve $\tau = f(\dot{\gamma})$ where $\dot{\gamma} > 1\ s^{-1}$ in agreement with the publication of the NIST (Olivas et al., 2017).

2.2.7. Scanning electron microscopy

The influence of LCLL and calcined LCLL on the microstructure of the cement paste. A cylindrical specimen of cement paste cured under water was sawed under cutting oil using a wheel saw to obtain a 1 mm thick slide. The slides were rinsed in isopropyl alcohol and immersed in 100 mL of isopropyl alcohol for 48 h. After this procedure, the samples were vacuum dried and vacuum impregnated with low viscosity epoxy resin to solidify the internal microstructure. To insure good quality BSE image, samples were first ground using a SiC paper of 600 grit and polished with 9 μm, 3 μm, 1 μm diamonds paste using deodorized petrol as a lubricant. To avoid contamination from previous polishing steps, the sample was cleaned in isopropyl alcohol using an ultrasonic cleaner after each step. The samples were a scanned with a Hitachi TM3030 tabletop SEM microscope equipped with a backscattered electron detector under an accelerating voltage of 15 kV.

2.2.8. R^3 thermodynamic modelling

Thermodynamic modelling was carried out using GEMS-PSI (Kulik et al., 2004) based on Gibbs energy minimization. This software allows to compute equilibrium speciation of dissolved species, the quantity and the composition of solid phases. The thermodynamics data for aqueous species and hydration products were respectively taken from the PSI-Nagra (Hummel et al., 2002) and CEMdata18 (Lothenbach et al., 2019). In this study, thermodynamic modelling was used to calculate the heat released based on calcium hydroxide consumption on the R^3 paste at 40°C with reactive silica, reactive alumina and inert materials. These models are respectively presented as CaO-SiO_2-KOH, CaO-Al_2O_3-KOH, and CaO-KOH systems.

3. Results

3.1. Mortar

The results of compressive strength and relative strengths Portland cement and Portland blended cements are respectively presented in Fig.2 and Fig.3. For each specimen tested, the relative compressive strength (RCS) was calculated from Eq. 6:

$$RCS = \frac{R_{100\ Cement}^{i\ days} - R_{20SCM}^{i\ days}}{R_{100\ cement}^{i\ days}} \qquad \text{Eq. (6)}$$

where $R_{100\ Cement}^{i\ days}$ and $R_{20SCM}^{i\ days}$ are respectively the compressive strength at i-days of the unblended cement reference and of blended cement with SCM.

As for a 20% replacement, a dilution effect appears and it is equivalent to an increase of the water to cement ratio from 0.485 to 0.610, which causes a reduction of compressive strength (Cyr et al., 2005; Li et al., 2018). This effect can be observed in the mortars containing inert materials like ground quartz (Q).

In this study, the addition of 20% of quartz causes a reduction of 20–30% in compressive strength from 1 to 112 days. Also, quartz mortar has a relative strength lower than 20%. When a pozzolanic or a latent hydraulic material is incorporated to blended cement, the increase of relative strengths above 20 % is attributed to the reaction of active phases to form more hydrated products.

According to Fig.2, silica fume exhibits highly reactive properties. Therefore, the compressive strength is always significantly higher than Portland cement. For GGBS, and (fly ashes), the

compressive strength results are similar or closer to Portland cement mix. However, these samples show some difference in relative compressive strength.

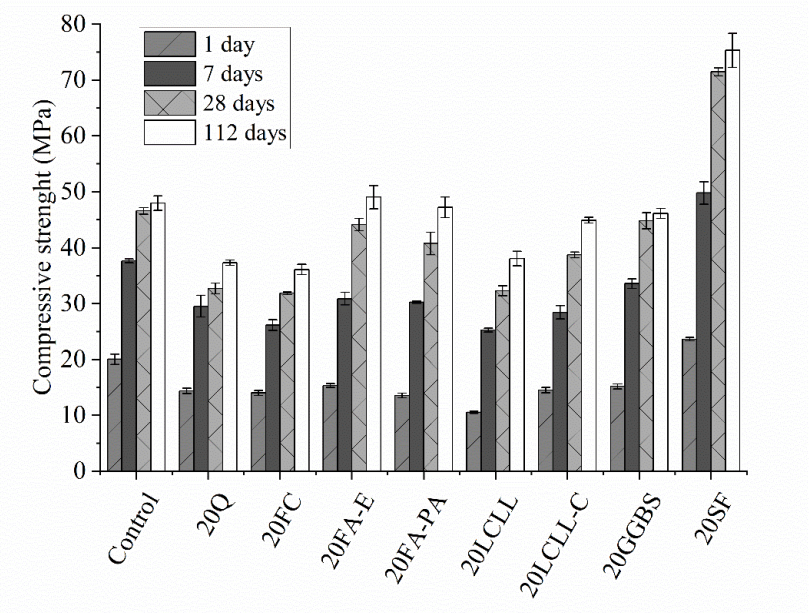

Figure 2:Compressive strength of mortar with 20% of SCM replacement at 1, 7 ,28 and 112 days (mean values and standard deviation bars).

As shown in Fig.3, the relative strength of GGBS is greater than all the other SCMs from 1 to 28 days. This difference is clearly visible at 7 and 28 days and then decreases at 112 days to reach a value equal or lower to other reactive SCMs. For the fly ashes (FA-E and FA-PA), an absence or a low reactivity is observed at 1 and 7 days. These reactivities are still lower than GGBS blended cement at 28 days, but, the reactivities are equivalent or higher than Portland cement and GGBS blended cement at 112 days due to the pozzolanic reactions. For inert SCMs like limestone filler, the compressive strength remains lower or equivalent to the compressive strength of quartz blended cement with a decrease around 20-25%, for all the days tested due to the dilution effect. Similar results were obtained by (Donatello et al., 2010; Li et al., 2018; Tironi et al., 2013).

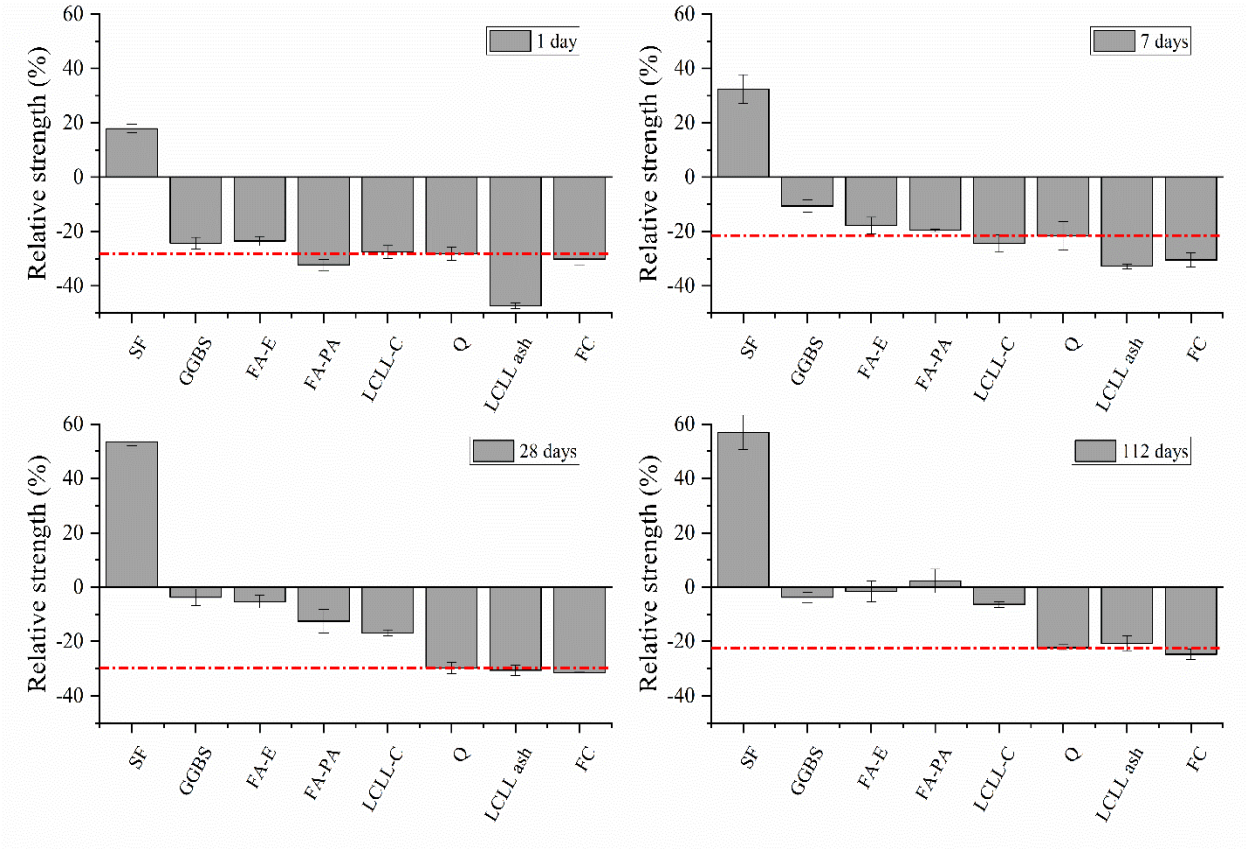

Figure 3:Relative compressive strength of mortar samples with SCM at 1, 7, 28 and 112 days. The red line refers to the quarts reference mortar sample.

Considering the results obtained with the other SCMs, it is possible to compare LCLL and calcined LCLL blended cement's reactivities. For calcined LCLL, the reactivity is closer to a low reactive fly ash, with inert behavior at 1 and 7 days and a reactivity lower or equivalent to a fly ash at 28 and 112 days. On the other hand, the LCLL shows an inert behavior in blended cement, similar to quartz from 28 to 112 days. Moreover, the results at 1 and 7 days for relative compressive strengths show a significant decrease of about 10% more than quartz blended cement. These results indicate a retarding effect of the LCLL on the hydration of cement in the first days, creating a delay on hydration at one and seven days. This delay is probably due to the presence of carbonaceous materials in LCLL as already observed for hydration of cement (Dutta et al., 1995) and fly ash (Wesche, 1991). For certain conditions, like concreting in hot weather, this retarding effect is beneficial.

3.2. Frattini

The results of the Frattini tests allow to calculate calcium reductions. These are calculated by considering the ratio of the vertical distance of data point to the lime solubility curve and from the lime solubility curve to the zero point at the given [OH^-]. The Europeans standard EN 196-5 (British Standard Euronorm, 2005) only provides $Ca(OH)_2$ solubility data at 40 °C for [OH^-] between 35 and 90 mmol/L. In this last [OH^-] range, the theoretical maximum [Ca^{2+}] concentration is calculated by using the formula given in the European's norm according to the Eq. 7:

$$[Ca^{2+}] = \frac{350}{[OH^-] - 15} \qquad \text{Eq. (7)}$$

The results (Fig.4a) indicate that samples containing 80% Portland cement and 20% of test SCM, show pozzolanic activity for FA, SF, whereas quartz (Q) and limestone filler (FC) are inactive.

For each SCM sample, the difference in calcium concentration was calculated for each sample between the theoretical maximum calcium removed from the EN-196 and the observed calcium concentration in the sample. The difference was then quantified as a percentage of the theoretical maximum (Fig.4b). These results confirm that quartz powder (Q), limestone filler (FC) and slag (GGBS) are not pozzolanic. Since the GGBS is a hydraulic binder, the low value of calcium removal for GGBS samples was expected, since this reaction did not consume calcium, as a pozzolanic reaction does (Suraneni et al., 2019).

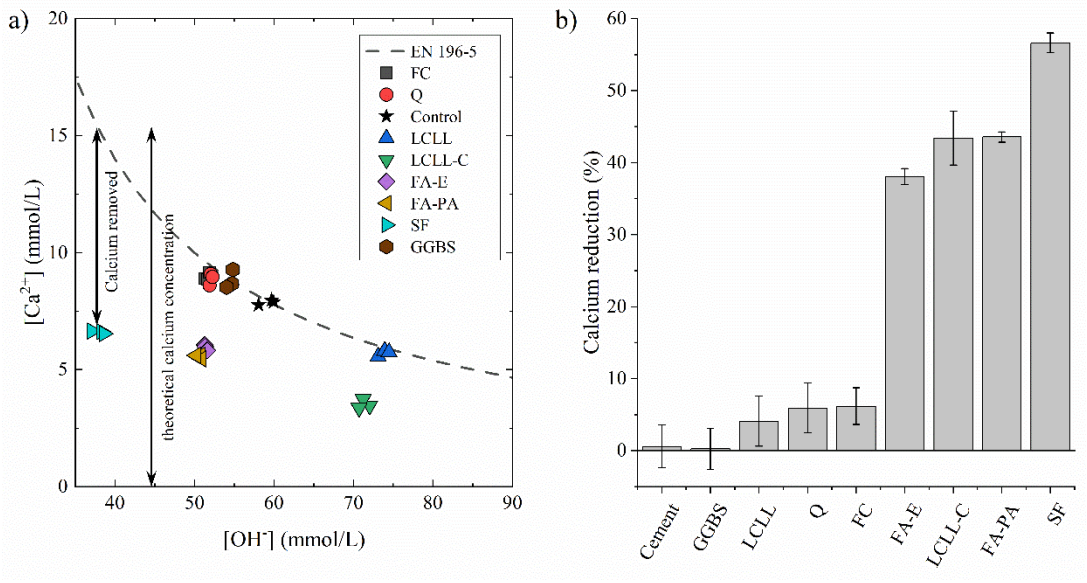

Figure 4:a) Frattini results for the different SCM studied. The dashed line refers to the max CaO content according to the EN-196-5 European standard and b) calcium reduction form Frattini test for each SCM tested.

A strong pozzolanic activity of silica fume (SF) with a 56% calcium removal and fly ashes (FA) with a calcium removal between 38 and 44%. These results are in agreement with others (Li et al., 2018; Suraneni et al., 2019; Suraneni and Weiss, 2017). As observed in a previous work (Donatello et al., 2010), some negative values were observed in particular for GGBS and control, which indicates filtration and/or experimental errors in the titration procedure during the sample preparation or titration. As they recommended, negative results for calcium reductions were normalized to 0 % equivalent calcium removal.

For the LCLL and the calcined LCLL (LCLL-C) the results are similar to the mortar test observation. With a low calcium reduction of 4%, unlike quartz and limestone filler, the LCLL fails to show a pozzolanic reactivity. However, the calcined LCLL shows a calcium reduction around 44%, similar to a fly ash. Moreover, the LCLL and calcined LCLL show a high concentration of hydroxyl ions, seen in Fig.4. This can be explained by the high concentration of soluble sodium ions from the LCLL in solution.

3.3.R^3: Heat release and calcium hydroxide consumption

Heat release is a great indicator of the presence of chemical reactivity since hydrated phases' precipitations are mainly exothermic reactions. Fig.5 shows the cumulative heat released and the lime consumption after 7 days at 40°C. However, beyond this time, the signal recorded by the isothermal calorimeter is hardly perceptible from the baseline. After 7 days, the silica fume shows the greatest heat released with 620 J/g of SCM, followed by the GGBS with 440 J/g, and the fly ashes around 247 J/g. The same type of result was obtained for the calcium hydroxide consumption, with values around 212, 70 and 80 g/100 g of SCM for the silica fume, GGBS and fly ashes respectively. GGBS showed a higher heat released than fly ashes despite a lower portlandite consumption. This consumption did not follow the pozzolanic pattern where heat released is expected to be proportional to portlandite consumption. It is then a characteristic of the hydraulic behavior of slag (Suraneni et al., 2019). The heat release and the calcium hydroxide consumption of limestone filler is extremely low due to its inert behavior. However, the quartz powder showed a significantly higher value than limestone filler, particularly for the calcium hydroxide consumption. Similar results for quartz were observed and are due to the greater solubility of quartz at 40°C and with a high pH from the R^3 paste composition (Li et al., 2018; Suraneni et al., 2019).

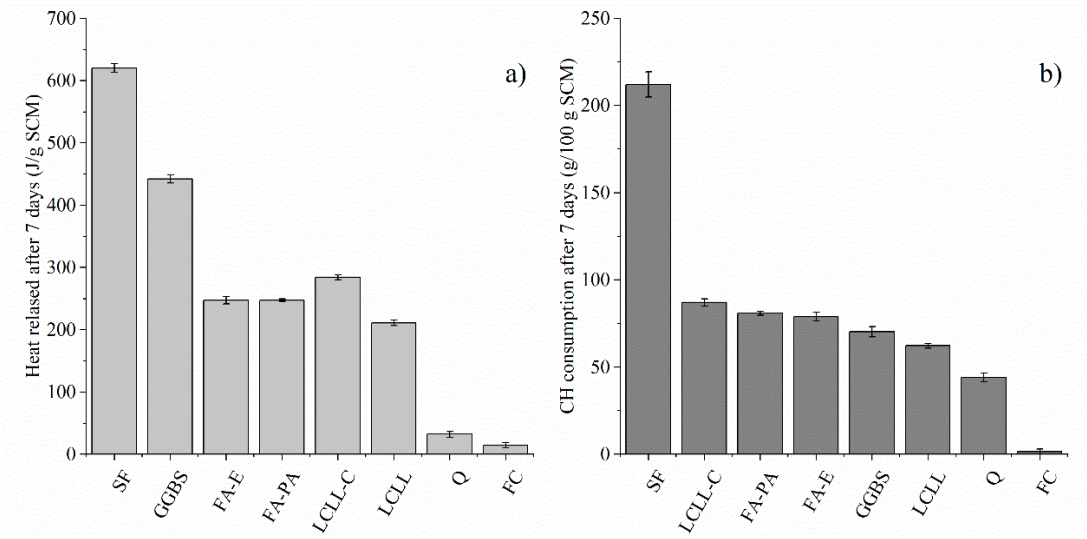

Figure 5 : (a) Heat release and (b) calcium hydroxide consumption after 7 days at 40°C.

The results for the LCLL were unexpectedly higher than limestone filler and quartz powder, with a heat release of 211 J/g and a portlandite consumption of 62 g/100 g. These results were similar

418 to a fly ash which contradicts the mortar and Frattini tests results. However, an expansion of the
419 paste was clearly visible on each R^3's replicate ampoules containing LCLL (Figure 12). This hints
420 for a hydro reactivity causing gas generation in the paste, at 40°C and high pH. On the other hand,
421 the calcined LCLL with a heat release of 284 J/g and the calcium hydroxide consumption of
422 87 g/100 g, showed reactivity slightly higher than fly ashes. In these R^3 samples, no expansion
423 was observed in the ampoules which indicates the absence of hydro reactivity and confirm the
424 reactivity of calcined LCLL. These results are consistent with mortar and Frattini tests.
425

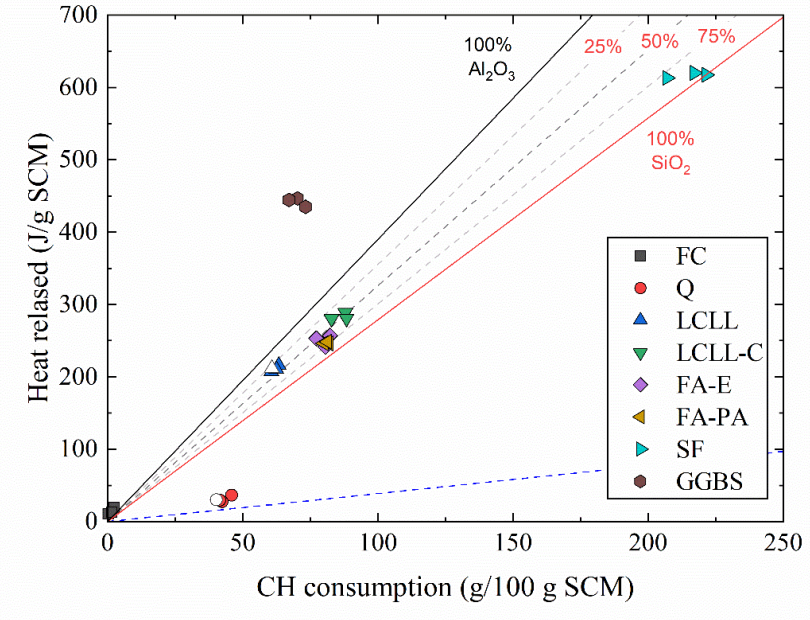

426
427 Figure 6 : R3 test heat released in function of the portlandite consumption for the SCM studied.
428
429 The grey, red, blue dashed lines refers respectively to the thermodynamically modelling of CaO-
430 SiO_2-KOH, CaO-Al_2O_3-KOH, and CaO-KOH systems calculating with GEMS-PSI.Fig.6 shows
431 the heat release versus calcium hydroxide consumption. According to (Suraneni et al., 2019), this
432 is a way to classify the tested materials according to their reactivity types known as: inert (quartz,
433 limestone), pozzolanic (fly ashes), highly pozzolanic (silica fume) and hydraulic (slag) materials.
434 For the CaO-SiO_2-KOH, CaO-Al_2O_3-KOH, and CaO-KOH systems, the thermodynamic
435 simulations with GEMS-PSI, respectively, give the following heats of reaction: 279 J/g, 390 J/g
436 and 3.9 J/g per grams of calcium hydroxide (respectively shown by the grey, red, blue dashed
437 lines). The red line represents the linear relationship between the heat released and portlandite

consumption for a pozzolanic sample only composed of pure reactive silica. In the same fashion, the grey line represents a pozzolanic sample only composed of pure reactive alumina describing the same tendency.

Thermodynamic modelling results are correlated with the experimental results for the R^3 paste on fly ashes and silica fume in function of the SiO_2 and Al_2O_3 composition. On Fig.6, the different reactive silica/reactive alumina ratios are represented with the grey dash lines. For fly ashes the reactive silica and alumina are estimated from the modelling around 75% silica and 25% alumina. These results are confirmed by the silica and alumina content in the raw composition (Table 1). In this case, the estimated proportion of reactive silica in calcined LCLL is approximately around 50%. The same reasoning can be applied to LCLL and shows a greater proportion of reactive alumina. However, the values for GGBS samples were not correlated with the thermodynamic modelling since the hydraulic behavior of slag was not simulated in this study with the thermodynamic modelling.

3.4. R^3: X-ray diffraction

Fig.7 shows the XRD diffractograms from the R^3 sample extract from the calorimeter ampoules after 7 days at 40°C. For each sample, the hydration reactions were stopped, when solvent exchange is completed. For inert materials, as quartz or limestone, the major phases are still portlandite (calcium hydroxide), calcite and quartz or limestone. Nonetheless, the silica fume samples showed portlandite peaks with a lower intensity, a bump around 30° 2θ and higher intensity from 5 to 7.5° 2θ. This indicates C-S-H formation by consumption of portlandite.

For slag, the presence of reactive alumina with sulfate and carbonate in the paste shows the formation of ettringite (AFt) and hemicarboaluminate (Hc) respectively by the peaks at 9° 2θ and 11° 2θ. Fly ashes show the formation of ettringite (AFt) and monocarboaluminate (Mc) respectively by the peaks at 9° 2θ and 11.7° 2θ (Hewlett et al., 2004; Lothenbach et al., 2007; Skibsted and Snellings, 2019). Similar results to fly ashes were observed with calcined LCLL, but with a stronger monocarboaluminate (Mc) peak intensity, indicating their higher concentration. However, LCLL shows new peaks between 10 and 11° 2θ but no ettringite was observed. These peaks are attributed to monosulfoaluminate (AFm) and hemicarboaluminate (Hc) phases which

contain alumina. In the R^3 paste, LCLL is the only alumina source which let's suppose that LCLL released alumina ions in solution in the test conditions (40°C).

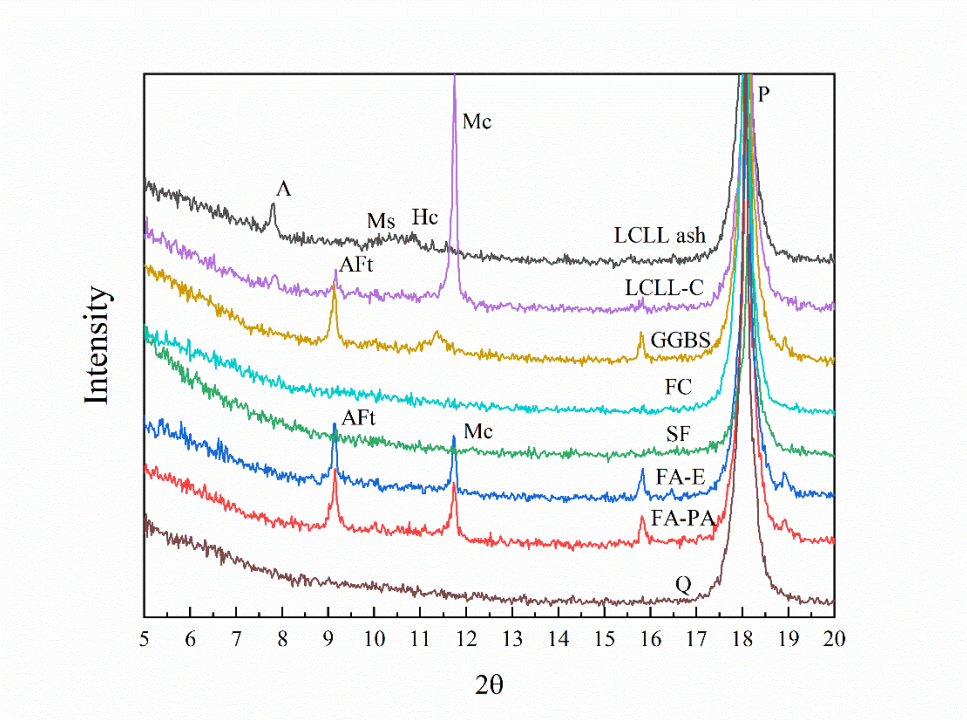

Figure 7 : XRD spectra on R3 mixes after solvent exchange hydration stoppage. (P:Porlandite, C:Calcite, Q:Quartz, AFt:Ettringite, Mc:Monocarboaluminate, Hc:Hemicarboaluminate).

For each R^3 mixes the crystalline compositions were measured by Rietveld analysis. Results are presented Fig.8. For inert materials, like the limestone filler, no consumption of portlandite was observed. On the other hand, samples containing quartz showed a low consumption of portlandite, and the formation of amorphous phases. This may also indicate the low reactivity of quartz to form C-S-H in R^3 experimental condition. Materials as fly ashes or slag containing reactive silica and alumina, show higher consumption of portlandite. Fly ashes showed an ettringite content around 3.2 to 3.4 g and monocarboaluminate from 2.3 to 3.1 g per 100 g of anhydrous. Slag showed an ettringite content of 3.4 g and hemicarboaluminate of 3.6 g per 100 g of anhydrous. The amorphous content measured in the slag and fly ash samples, also show an increase between 17 g to 28 g per 100 g of anhydrous. However, these values contain the new amorphous phases formed, as C-S-H, but composed in the majority of unreacted SCM. For samples with silica fume, a higher consumption of portlandite and an important formation of amorphous phases are observed. This

indicates a high reactivity with portlandite to form C-S-H which here, compose the major part of the amorphous phases (Scrivener et al., 2016).

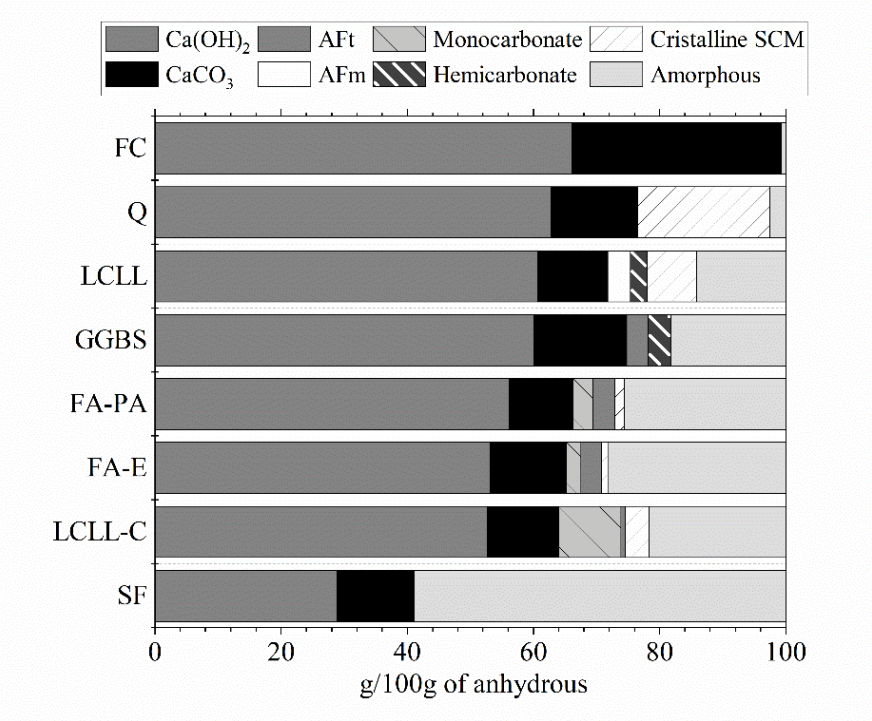

Figure 8 : R3 mixes composition from quantitative PXRD results after solvent exchange hydration stoppage.

The calcined LCLL samples show a similar trend to fly ashes with a lower ettringite content and a higher monocarboaluminate content. The decrease of ettringite is explained by the high pH of the solution due to soluble alkalis from calcined LCLL. These conditions favored the solubility of carbonates and the precipitation of carbonate phases (Dow and Glasser, 2003). Moreover, even though calcination at high temperature treatment was applied, some stable phases remain hardly reactive, such as corundum or quartz which limits the amount of amorphous generated. Indeed, a lower level of amorphous was observed due to a lower level of reactive silica and alumina in calcined LCLL at 1050°C, as (Wang et al., 2017).

For LCLL, the consumption of portlandite and the formation of new phases, such as monosulfoaluminate and hemicarboaluminate, seen on the R^3 test results, are indicators of the possible reactivity of LCLL. However, by considering the crystalline part detected and the amorphous content of LCLL, new amorphous phases, like C-S-H, were not significantly present.

This indicates the inert behavior of silicate phases of LCLL as albite or nepheline. The presence of phases containing alumina tends to confirm the hydro reactivity of LCLL in the R^3 test conditions which released ions containing alumina (Kimmerle et al., 1993; Øye, 2017).

An iterative thermodynamic simulation was realized from the quantitative XRD data, to evaluate the reaction percentage of LCLL, and validate the observed results from R^3 tests. According to the simulations in the R^3 conditions, 13% of LCLL reacted during the R^3 test. This result is represented by the white triangle on Fig.6. This tends to confirm the unexpected reactivity of LCLL during the R^3 test due to the hydro reactivity. Moreover, to validate the process, the same modelling was repeated for the quartz R^3 sample. The result showed a reaction of quartz about 6%, which is represented by the white dot the Fig.6.

3.5. Mercury intrusion porosimetry

The Fig. 9 presents the results from mercury intrusion into cement pastes. In order to limit the number of trials, the second fly ash (FA-PA) has not been tested. Different porosity and critical pore radius values are observed for the different SCMs. The critical pore radius is defined by the inflection point of the main intrusion seen in the cumulative intrusion curb from raw MIP data. This critical pore radius also appears as the main peak on the differential pore size distribution (Scrivener et al., 2016).

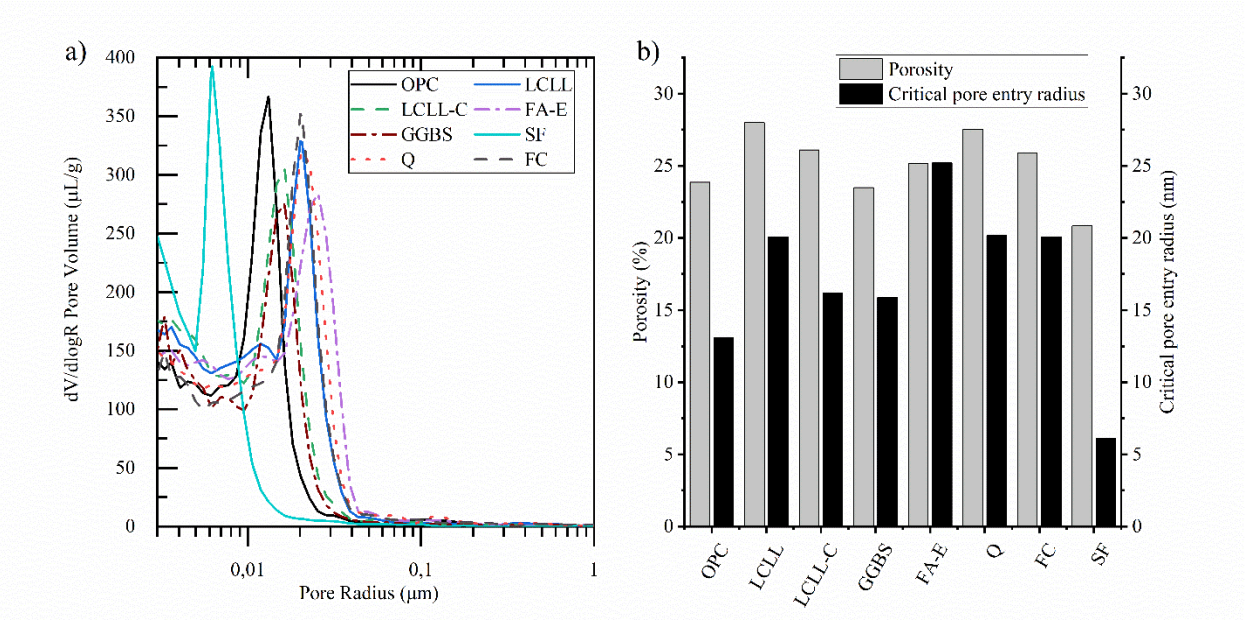

Figure 9 : a) MIP differential pore size distribution and b) porosity and critical pore radius for the different SCMs tested.

For the Portland cement and the GGBS, the porosities are respectively of 23.9 % and 23.5 %. However, the critical pore radius is smaller for OPC than GGBS as seen in (Chen et al., 2013; Lin et al., 2018). The silica fume shows a lower porosity than cement, around 21% with a pore entry radius of less than 7 nm. Very similar to the literature (Duan et al., 2013; Feldman and Cheng-Yi, 1985; Poon et al., 1999). The fly ash tested shows greater porosity than the previous around 25% with a critical pore entry radius of 25 nm again, in a similar trend to the literature (Poon et al., 1999; Yu et al., 2017) . Moreover, the limestone filler and the quartz powder show porosities of 26 % and 27 % respectively with a similar critical pore entry radius around 20 nm. Similar to the literature (Elgalhud et al., 2016; Lin et al., 2018; Panesar and Francis, 2014). LCLL stands out by having the highest porosity of 28% with a critical pore entry radius similar to limestone and quartz filler. In contrast, calcined LCLL has a slightly lower porosity than LCLL with 26 % and a similar critical pore radius of 15 nm to GGBS. This shows that the pore diameter of the calcined LCLL mixture is smaller than for the LCLL mixture. However, in the two mixtures containing LCLL or calcined LCLL, the observed porosity is greater than that of Portland cement.

3.6. Rheology

The rheological properties were measured for each mix of cement paste. Fig.10 presents the measures in plastic viscosity and the yield stress obtained by a geometric spindle mounted on a rheometer. The measures of LCLL and LCLL-C are compared to Portland cement and other SCMs mixes. OPC shows a plastic viscosity and stress yield of 0.25 Pa.s and 27 Pa respectively. Silica fume shows a plastic viscosity and yield stress greater than all other mixes with 0.38 Pa.s and 72 Pa , as expected due to the size of its particles (Ferraris et al., 2001; Vikan and Justnes, 2007) . Except for SF and LCLL mixes, all SCMS mixes tested showed lower or equivalent rheological properties to OPC. Limestone filler shows a plastic viscosity and yield stress of 0.11 Pa.s and 27 Pa respectively, consistent with the literature (Svermova et al., 2003; Vikan and Justnes, 2007). Quartz filler has a plastic viscosity of 0.25 Pa.s , similar to cement, but a yield stress inferior to OPC with 21 Pa. Since the yield stress is related to a Power law to flow (Charrier and Ouellet-Plamondon, 2020; Roussel, 2012) it is expected that its decrease is linked to a greater flow, which was also observed after the addition of quartz powder in mixes (Lin et al., 2018; Tavares et al., 2020). Adding fly ash or GGBS show a decrease in plastic viscosity, with respectively 0.29, 0.20 and 0.20 for FA-E, FA-PA and GGBS as previously seen in the literature (Jiang et al., 2020; Thiyagarajan et al., 2018). Here, the LCLL has a plastic viscosity similar to cement and quartz powder with 0.25 Pa.s. However, its yield stress is higher than other cement and SCMs mixes, with 30 Pa this suggests that adding LCLL would increase the flow due to its higher content in graphite which increases its water demand. This has also been observed in fly ashes: since FA-E has a greater LOI than FA-PA it also has a greater yield stress due to its high carbonaceous content. This is also confirmed by LCLL-C which has a yield stress of 22 Pa. After calcination it has a lower LOI which entails a lower yield stress. Moreover, its plastic viscosity is also the lowest observed, with 0.1 Pa.s.

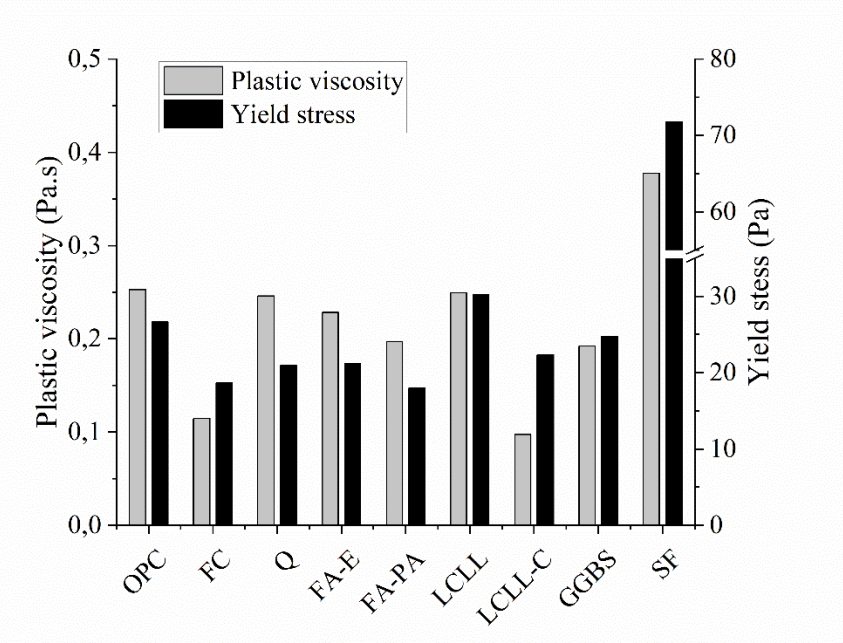

Figure 10 : Plastic viscosity and yield stress on the cement paste.

3.7.SEM-BSE

Samples of cement pastes containing 20% LCLL and 20% LCLL-C were observed at 28 days and 1 year. The Fig. 12 presents BSE scanning electron images of LCLL and LCLL-C grains. After 28 days, the grains of LCLL-C and LCLL show no signs of hydration. It is important to note the difference in shape between the grains of LCLL and calcined LCLL. The grains of LCLL are heterogeneous composed of the different phases of the LCLL while the grains of LCLL calcined are grains comprising several phases fused together. After 1 year, the grains of LCLL partially hydrated are observed in the periphery while the grains of LCLL calcined are fully hydrated with the exception of the corundum grains which compose it. Moreover, no portlandite was observed around the hydrated calcined LCLL grain, suggesting a pozzolanic reaction. This confirms the low reactivity of LCLL even after 1 year and the increase in reactivity of LCLL after calcination at 1050 ° C.

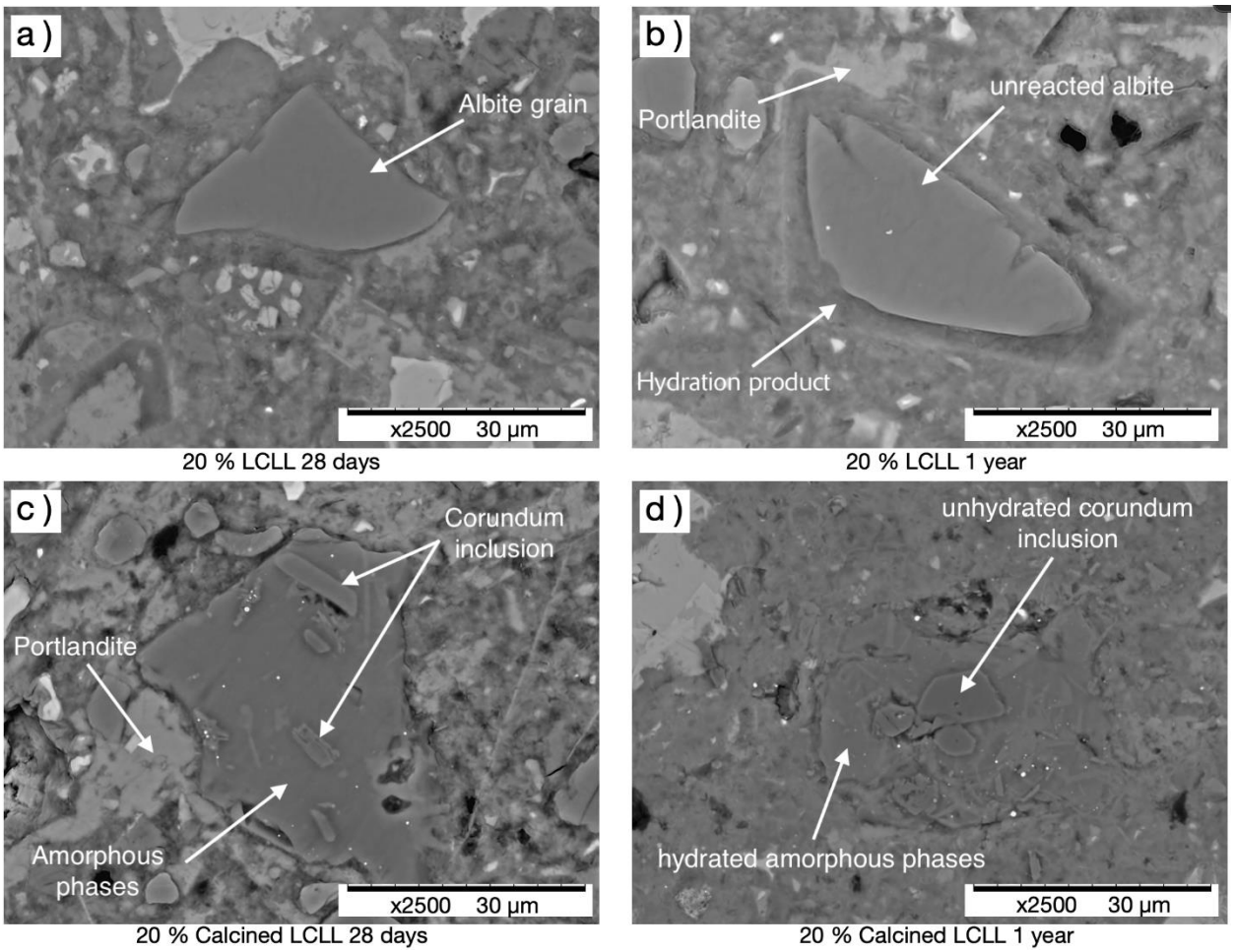

Figure 11 : SEM BSE observation of LCLL and LCLL grains after 28 days and 1 year of hydration.

4. Discussion

4.1.LCLL reactivity

According to the previous mortar and Frattini tests, the reactivity of LCLL can be considered equivalent to an inert material in cement, similar to quartz. This result was expected since important quantities of low reactivity phases composed LCLL, such as corundum, quartz, albite and nepheline. The SEM observation of LCLL also confirms the low reactivity of LCLL grains in cement after 1 year. Moreover, the SEM observation shows LCLL monophasic grains with angular edges. The lower compressive strength of the early age of hydration observed on mortars can be explained by the presence of carbonaceous materials in LCLL. Similar effects were observed by

(Dutta et al., 1995). However, as observed on MIP results, the porosity and the critical pore radius are more important in LCLL containing cement paste which explains the lower compressive strength (Chen et al., 2013). Moreover, hydro reactivity occurred during R^3 tests due to its higher temperature increase necessary for improving kinetics of pozzolanic reactions. This turn LCLL into reactive material. From the crystalline part detected by XRD and the raw composition of LCLL, it is possible to calculate the remaining LCLL content in the R^3 paste after 7 days. This result gives a LCLL content about 19% and a new amorphous material about 2.5%. This result is similar to quartz powder and indicates the inert behavior of silicate phases of LCLL such as albite or nepheline. The presence of phases containing alumina tends to confirm the hydro reactivity of LCLL in the R^3 test conditions by releasing ions containing alumina (Kimmerle et al., 1993; Øye, 2017). This hypothesis seems to be consistent with the Fig.7 of R^3 results for LCLL, where the phases induced by the hydro reactivity seem to show a higher proportion of reactive alumina. These reactions are followed by the generation of gases in the paste, which engenders paste expansion (Fig. 12). However, in this study, no expansion was observed on mortar specimens. Temperature and chemistry, particularly pH, are key parameters to induce hydro reactivity and expansion. A low hydro reactivity can explain the higher porosity in cement, however other parameters as the higher carbonaceous material content or the particle shape can also affect the porosity. Among the previous possibilities, carbonaceous material presence would explain better the higher porosity in LCLL containing mixes. Such results were also observed with FA-E MIP results. The carbonaceous material content also entails change on the rheological behavior of mix containing LCLL. The presence of a high content of graphite might have increased the yield stress and the viscosity of cement paste, but the high concentration of LCLL in free alkali, in particular sodium, can also explain this observation (Grzeszczyk and Kucharska, 1990). Moreover, the shape of LCLL grains explains the difference of rheological behavior between LCLL and fly ash. With an angular shape LCLL grains tends to increase the yields stress and the plastic viscosity. A contrary, rounded fly ash particles tend to decreased the same properties (Aïtcin and Flatt, 2015). Consequently, we can expect that mixes containing LCLL will have a greater water demand and a smaller slump or flow.

Figure 12 : Ampoules of R3 samples with LCLL (right) and calcined LCLL (left) after 7 days testing.

In these conditions, the use of LCLL as SCM can be motivated by an alternative stabilization in concrete as a filler. In this context, optimized packing method can make it useful. However, further tests must be done to confirm the absence of hydro reactivity or durability concerns with the cement, water and aggregates used.

4.2. Calcined LCLL reactivity

Calcination appears as an interesting solution to improve the reactivity of LCLL in cement. In R^3, Frattini, and mortar test calcined LCLL shows reactivity similar to a fly ash. However, the result in compressive strength shows a lower efficiency than fly ash.. This efficiency difference was explained by the higher crystalline phase content and the lower quantity of reactive silica in calcined LCLL. But this lack of silica could be compensated by a higher concentration of reactive alumina which allows the precipitation of additional aluminate phases to densify the cementitious matrix. This is confirmed by MIP results showing a lower porosity and a lower critical pore diameter indicating a smaller porosity size than uncalcined LCLL. SEM observation also confirms the higher reactivity of calcined LCLL with almost complete reacted grains. In contrast to uncalcined LCLL, the LCLL-C grains contains different melted phases which enhances the reactivity of the grains with more chemical species available. In terms of chemical composition, the calcined LCLL is closer to calcined clay. As previously studied on calcined clay, the addition

649 of sulfate or carbonates allow the formation of new phases as ettringite, monocarboaluminate and
650 hemicarboaluminate (Avet et al., 2016).
651
652 This effect was clearly visible on the R^3 test for calcined LCLL with ettringite and
653 monocarboaluminate. In comparison to fly ashes, calcined LCLL showed a higher formation of
654 monocarboaluminate. This preferential precipitation occurs in R^3 mixes due to both the high
655 CO_3/SO_4 ratio in the paste and the higher pH of the solution caused by the alkalis released by
656 LCLL (Dow and Glasser, 2003; Feng et al., 2016; Palomo, 2012). Moreover, the calcination
657 cancelled the delay on compressive strength in the early days of hydration observed with raw
658 LCLL. This observation tends to confirm the effect of carbonaceous residues in LCLL on the
659 setting time as already observed with fly ash blended cement (Wesche, 1991). The decreased of
660 carbonaceous residues in LCLL-C also demonstrate lower yield stress and plastic viscosity, which
661 indicate a lower water demand. However, the very low plastic viscosity of LCLL-C can entail
662 some concern about segregation in concrete, in particular with big aggregate (Roussel, 2012). The
663 high alkali content of LCLL is a significant advantage, since it decreases the liquid formation
664 temperature and the energy needed for calcination (Wang et al., 2017). This allows the formation
665 at high temperature of glass materials rich in sodium similar to soda-lime glass already use in
666 cement (Shi and Zheng, 2007).
667
668 The calcination improves significantly the reactivity of LCLL and allows a possible use in concrete
669 as a reactive SCM to replace a part of cement. However, high temperature calcination requires
670 specific industrial processes with higher energetic, environmental and financial impacts. With a
671 lower calcination temperature than cement, the replacement of a part of cement by calcined LCLL
672 could reduce the same previously stated impacts. Moreover, incorporating calcined LCLL and its
673 important reactive alumina amount to models based on calcined clay limestone cement as LC3 by
674 additions of non-calcined carbonates or sulfate. These cements could further reduce the
675 environment and energetic impacts without affecting the blended cement performance (Scrivener
676 et al., 2018). Further investigations must be done to evaluate the real environment and energetic
677 impacts of calcined LCLL in cement.

5. Conclusion

Based on the presented results, the following concluding remarks can be drawn:

a) The valorization of treated SPL in cementitious materials, offers new opportunities for aluminum and cement industries to decrease the environmental impact of their materials by reusing a local waste and avoiding landfill.

b) LCLL is not reactive in cement. Hydro reactivity and expansion due to gas generation can happen depending on the chemistry or the temperature of hydration of the binder. This hydro reactivity releases aluminates in solution which precipitates aluminates phases conferring to LCLL a low reactivity.

c) Use of LCLL as filler in cement is possible. However, to avoid expansion or durability concerns, preliminary tests must be realized to evaluate the compatibility of LCLL with cement, aggregates and water. Moreover, the presence of graphite in uncalcined LCLL tends to entail delay in the setting time.

d) The calcination of LCLL at 1050°C significantly improves the reactivity in cement. Calcined LCLL reactivity shows similarities to a calcined clay with highly reactive alumina. Hydro reactivity concerns are not observed with calcined LCLL due to the high temperature destruction, evaporation or incorporation in new phases, of hydro-reactive compounds. More investigation of the reactivity of LCLL with temperature is needed.

e) The replacement of a part of cement by calcined LCLL could reduce the environmental and energetic impacts of blended cement. This lower impact of LCLL is due to its lower calcination temperature than cement and the valorization of a treated hazardous material.

f) More investigation will be done to understand the conditions which lead hydro-creativity and its impact on durability. For calcined LCLL, more investigation must be done to evaluate the chemistry and aluminum incorporation in hydrated cement phases such as C-S-H.

Acknowledgments

The authors are grateful to NSERC CRD grant program (CRDPJ 515485 – 17), CRITM consortium, Rio Tinto and Ciment Québec Inc. for their financial support for this project.

References

Abell, A.B., Willis, K.L., Lange, D.A., 1999. Mercury intrusion porosimetry and image analysis of cement-based materials. J. Colloid Interface Sci. 211, 39–44. https://doi.org/10.1006/jcis.1998.5986

Agrawal, A., Sahu, K.K., Pandey, B.D., 2004. Solid waste management in non-ferrous industries in India. Resour. Conserv. Recycl. 42, 99–120. https://doi.org/10.1016/j.resconrec.2003.10.004

Aïtcin, P.C., Flatt, R.J., 2015. Science and technology of concrete admixtures, Science and Technology of Concrete Admixtures. https://doi.org/10.1016/C2015-0-00150-2

Ambroise, J., Murat, M., Péra, J., 1985. Hydration reaction and hardening of calcined clays and related minerals V. Extension of the research and general conclusions. Cem. Concr. Res. 15, 261–268. https://doi.org/10.1016/0008-8846(85)90037-7

Andrew, R.M., 2019. Global CO2 emissions from cement production , 1928 – 2018. Earth Syst. Sci. Data 11, 1675–1710. https://doi.org/https://doi.org/10.5194/essd-11-1675-2019

ASTM International, 2016. C109/C109M − 16a Standard Test Method for Compressive Strength of Hydraulic Cement Mortars Using 2-in . or [50-mm] Cube Specimens). ASTM Stand. B. 1–9. https://doi.org/10.1520/C0109

ASTM International, 2015. C305 − 14 Standard Practice for Mechanical Mixing of Hydraulic Cement Pastes and Mortars. ASTM Stand. B. 14–16. https://doi.org/10.1520/C0305-14.2

ASTM International, 2014. C1738/C1738M-18 Standard Practice for High-Shear Mixing of Hydraulic Cement Pastes. ASTM Stand. B. 11–13. https://doi.org/10.1520/C1738-11A.2

ASTM International, 2010. C230/C230M − 14 Standard Specification for Flow Table for Use in Tests of Hydraulic Cement. ASTM Stand. B. 4–9. https://doi.org/10.1520/C0230

Avet, F., Snellings, R., Alujas, A., Ben, M., Scrivener, K., 2016. Cement and Concrete Research Development of a new rapid , relevant and reliable (R 3) test method to evaluate the pozzolanic reactivity of calcined kaolinitic clays. Cem. Concr. Res. 85, 1–11. https://doi.org/10.1016/j.cemconres.2016.02.015

Birry, L., Leclerc, S., Poirier, S., 2016. the Lcl & L Process : a Sustainable Solution for the Treatment and Recycling of Spent Potlining 467–472.

British Standard Euronorm, 2005. EN196: Methods of testing cement. Part 5: pozzolanicity test for pozzolanic cement.

Broek, S., Øye, H.A., 2018. Fundamentals of Managing Spent Potlining (SPL). Trav. 46, Proc. 35th Int. ICSOBA Conf. 817–834.

Cancio Díaz, Y., Sánchez Berriel, S., Heierli, U., Favier, A.R., Sánchez Machado, I.R., Scrivener, K.L., Martirena Hernández, J.F., Habert, G., 2017. Limestone calcined clay cement as a low-carbon solution to meet expanding cement demand in emerging economies. Dev. Eng. 2, 82–91. https://doi.org/10.1016/j.deveng.2017.06.001

Charrier, M., Ouellet-Plamondon, C., 2020. Testing Procedures on Materials to Formulate the Ink for 3D Printing. Transp. Res. Rec. 2674, 21–32. https://doi.org/10.1177/0361198120907583

Chen, X., Wu, S., Zhou, J., 2013. Influence of porosity on compressive and tensile strength of cement mortar. Constr. Build. Mater. 40, 869–874. https://doi.org/10.1016/j.conbuildmat.2012.11.072

Cyr, M., Lawrence, P., Ringot, E., 2005. Mineral admixtures in mortars Quantification of the physical effects of inert materials on short-term hydration 35, 719–730. https://doi.org/10.1016/j.cemconres.2004.05.030

Dhandapani, Y., Sakthivel, T., Santhanam, M., Gettu, R., Pillai, R.G., 2018. Mechanical properties and durability performance of concretes with Limestone Calcined Clay Cement (LC3). Cem. Concr. Res. 107, 136–151. https://doi.org/10.1016/j.cemconres.2018.02.005

Diamond, S., 2000. Mercury porosimetry An inappropriate method for the measurement of pore size distributions in cement-based materials. Cem. Concr. Res. 30, 1517–1525. https://doi.org/10.1016/S0008-8846(00)00370-7

Donatello, S., Tyrer, M., Cheeseman, C.R., 2010. Comparison of test methods to assess pozzolanic activity. Cem. Concr. Compos. 32, 121–127. https://doi.org/10.1016/j.cemconcomp.2009.10.008

Dow, C., Glasser, F.P., 2003. Calcium carbonate efflorescence on Portland cement and building materials. Cem. Concr. Res. 33, 147–154. https://doi.org/10.1016/S0008-8846(02)00937-7

Duan, P., Shui, Z., Chen, W., Shen, C., 2013. Effects of metakaolin, silica fume and slag on pore structure, interfacial transition zone and compressive strength of concrete. Constr. Build. Mater. 44, 1–6. https://doi.org/10.1016/j.conbuildmat.2013.02.075

Dutta, D.K., Bordoloi, D., Borthakur, P.C., 1995. Hydration of portland cement clinker in the presence of carbonaceous materials. Cem. Concr. Res. 25, 1095–1102.

https://doi.org/10.1016/0008-8846(95)00104-K
Elgalhud, A.A., Dhir, R.K., Ghataora, G., 2016. Limestone addition effects on concrete porosity. Cem. Concr. Compos. 72, 222–234. https://doi.org/10.1016/j.cemconcomp.2016.06.006
Fares, G., 2008. Nouveau systeme cimentaire : cas de la Fritte de verre. These de doctorat présenté en Juillet 2008, Université de Sherbrooke. https://doi.org/10.1177/001088048102200214
Favier, A., Scrivener, K., 2018. Alkali silica reaction and sulfate attack: Expansion of limestone calcined clay cement. RILEM Bookseries 16, 165–169. https://doi.org/10.1007/978-94-024-1207-9_26
Feldman, R.F., Cheng-Yi, H., 1985. Properties of portland cement-silica fume pastes I. Porosity and surface properties. Cem. Concr. Res. 15, 765–774. https://doi.org/10.1016/0008-8846(85)90141-3
Feng, P., Miao, C., Bullard, J.W., 2016. Factors Influencing the Stability of AFm and AFt in the Ca – Al – S – O – H System at 25 ° C. J. Am. Ceram. Soc. 1041, 1031–1041. https://doi.org/https://dx.doi.org/10.1111%2Fjace.13971
Ferraris, C.F., Obla, K.H., Hill, R., 2001. The influence of mineral admixtures on the rheology of cement paste and concrete. Cem. Concr. Res. 31, 245–255. https://doi.org/10.1016/S0008-8846(00)00454-3
Ferraris, C.F., Stutzman, P.E., Guthrie, W.F., Winpigler, J., 2015. Certification of SRM 2492 : Bingham Paste Mixture for Rheological Measurements, NIST Special Publication 260-174.
Gallé, C., 2001. Effect of drying on cement-based materials pore structure as identified by mercury intrusion porosimetry - A comparative study between oven-, vacuum-, and freeze-drying. Cem. Concr. Res. 31, 1467–1477. https://doi.org/10.1016/S0008-8846(01)00594-4
Gomes, V., Drumond, P.Z., Neto, J.O.P., Lira, A.R., 2005. Co-Processing at Cement Plant of Spent Potlining from the Aluminum Industry. Essent. Readings Light Met. Electrode Technol. Alum. Prod. https://doi.org/10.1002/9781118647745.ch142
Grzeszczyk, S., Kucharska, L., 1990. Hydrative reactivity of cement and rheological properties of fresh cement pastes. Cem. Concr. Res. 20, 165–174. https://doi.org/10.1016/0008-8846(90)90069-A
Hewlett, P.C., Bensted, J., Blezard, R.G., Brown, B., Capmas, A., Edmeades, R.M., Eglinton, M., Fidjestel, P., Glasser, F.P., Jackson, P., JLachowski, E.E., Lewis, R., Macphee, D.E.,

Massazza, F., Micheline, M.-R., Odler, I., Scrivener, K.L., Sims., I., 2004. Lea's Chemistry of Cement and Concrete, Lea's Chemistry of Cement and Concrete. https://doi.org/10.1016/B978-075066256-7/50024-2

Hummel, B.W., Berner, U., Curti, E., Pearson, F.J., Thoenen, T., 2002. Nagra / PSI Chemical Thermodynamic Data Base 01 / 01 813, 805–813.

Jawi, M. Al, Chow, C.M., Pujari, S., Pan, M., Kulkarni, T., Mahmoud, M., Akasha, H., Abdulla, S., 2020. Environmental Benefits of Using Spent Pot Lining (SPL) in Cement Production, Minerals, Metals and Materials Series. Springer International Publishing. https://doi.org/10.1007/978-3-030-36408-3_172

Jiang, D., Li, X., Lv, Y., Zhou, M., He, C., Jiang, W., Liu, Z., 2020. Utilization of limestone powder and fly ash in blended cement : Rheology , strength and hydration characteristics. Constr. Build. Mater. 232, 117228. https://doi.org/10.1016/j.conbuildmat.2019.117228

Kajaste, R., Hurme, M., 2016. Cement industry greenhouse gas emissions - Management options and abatement cost. J. Clean. Prod. 112, 4041–4052. https://doi.org/10.1016/j.jclepro.2015.07.055

Kimmerle, F.M., Bernier, J.-L., Kasireddy, V.K., Holywell, G., 1993. Chemical Revovery from Spent PotLining. Miner. Met. Mater. Soc. 671–685.

Kulik, D., Berner, U.R., Curti, E., 2004. Modeling chemical equilibrium partitioning with the GEMS-PSI code. PSI Sci. Rep. 2003 / Vol. IV, Nucl. Energy Saf. IV, 109–122.

Laldji, S., Tagnit-Hamou, A., 2016. Glass frit concrete as an alternative cementitious material. [WWW Document]. URL https://www.researchgate.net/publication/268294095%0AGLASS

Le Quéré, C., Moriarty, R., Andrew, R.M., Peters, G.P., Ciais, P., Friedlingstein, P., Jones, S.D., Sitch, S., Tans, P., Arneth, A., Boden, T.A., Bopp, L., Bozec, Y., Canadell, J.G., Chini, L.P., Chevallier, F., Cosca, C.E., Harris, I., Hoppema, M., Houghton, R.A., House, J.I., Jain, A.K., Johannessen, T., Kato, E., Keeling, R.F., Kitidis, V., Klein Goldewijk, K., Koven, C., Landa, C.S., Landschützer, P., Lenton, A., Lima, I.D., Marland, G., Mathis, J.T., Metzl, N., Nojiri, Y., Olsen, A., Ono, T., Peng, S., Peters, W., Pfeil, B., Poulter, B., Raupach, M.R., Regnier, P., Rödenbeck, C., Saito, S., Salisbury, J.E., Schuster, U., Schwinger, J., Séférian, R., Segschneider, J., Steinhoff, T., Stocker, B.D., Sutton, A.J., Takahashi, T., Tilbrook, B., Van Der Werf, G.R., Viovy, N., Wang, Y.P., Wanninkhof, R., Wiltshire, A., Zeng, N.,

2015. Global carbon budget 2014. Earth Syst. Sci. Data 7, 47–85. https://doi.org/10.5194/essd-7-47-2015

Lehne, J., Preston, F., 2018. Making Concrete Change- Innovation in Low-carbon Cement and Concrete.

Li, C., Ideker, J.H., Drimalas, T., 2015. The efficacy of calcined clays on mitigating alakli-silica reaction (ASR) in mortar and its influence on microstructure. RILEM Bookseries 10, 211–217. https://doi.org/10.1007/978-94-017-9939-3_26

Li, X., Snellings, R., Antoni, M., Alderete, N.M., Ben Haha, M., Bishnoi, S., Cizer, Ö., Cyr, M., De Weerdt, K., Dhandapani, Y., Duchesne, J., Haufe, J., Hooton, D., Juenger, M., Kamali-Bernard, S., Kramar, S., Marroccoli, M., Joseph, A.M., Parashar, A., Patapy, C., Provis, J.L., Sabio, S., Santhanam, M., Steger, L., Sui, T., Telesca, A., Vollpracht, A., Vargas, F., Walkley, B., Winnefeld, F., Ye, G., Zajac, M., Zhang, S., Scrivener, K.L., 2018. Reactivity tests for supplementary cementitious materials: RILEM TC 267-TRM phase 1. Mater. Struct. Constr. 51. https://doi.org/10.1617/s11527-018-1269-x

Lin, R.-S., Wang, X.-Y., Zhang, G.-Y., 2018. Effects of Quartz Powder on the Microstructure and Key Properties of Cement Paste. Sustainability 10, 3369. https://doi.org/10.3390/su10103369

Lothenbach, B., Kulik, D.A., Matschei, T., Balonis, M., Baquerizo, L., Dilnesa, B., Miron, G.D., Myers, R.J., 2019. Cemdata18: A chemical thermodynamic database for hydrated Portland cements and alkali-activated materials. Cem. Concr. Res. 115, 472–506. https://doi.org/10.1016/j.cemconres.2018.04.018

Lothenbach, B., Winnefeld, F., Alder, C., Wieland, E., Lunk, P., 2007. Effect of temperature on the pore solution, microstructure and hydration products of Portland cement pastes. Cem. Concr. Res. 37, 483–491. https://doi.org/10.1016/j.cemconres.2006.11.016

Ma, H., 2014. Mercury intrusion porosimetry in concrete technology: tips in measurement, pore structure parameter acquisition and application. J. Porous Mater. 21, 207–215. https://doi.org/10.1007/s10934-013-9765-4

Mather, B., 1958. The Partial Replacement of Portland Cement in Concrete, in: Cement and Concrete. ASTM International, 100 Barr Harbor Drive, PO Box C700, West Conshohocken, PA 19428-2959, pp. 37-37–38. https://doi.org/10.1520/stp39461s

Miller, S.A., John, V.M., Pacca, S.A., Horvath, A., 2018. Carbon dioxide reduction potential in

the global cement industry by 2050. Cem. Concr. Res. 114, 115–124. https://doi.org/10.1016/j.cemconres.2017.08.026

Mindess, S., Young, J.F., Darwin, D., 2003. Concrete, Second Ed. ed. Pearson Education, Inc.

Moro, F., Böhni, H., 2002. Ink-bottle effect in mercury intrusion porosimetry of cement-based materials. J. Colloid Interface Sci. 246, 135–149. https://doi.org/10.1006/jcis.2001.7962

Moukwa, M., Aitcin, P.C., 1988. The effect of drying on cement pastes pore structure as determined by mercury porosimetry. Cem. Concr. Res. 18, 745–752. https://doi.org/10.1016/0008-8846(88)90098-1

Murat, M., 1983. Hydration reaction and hardening of calcined clays and related minerals. I. Preliminary investigation on metakaolinite. Cem. Concr. Res. 13, 259–266. https://doi.org/10.1016/0008-8846(83)90109-6

Natural Resources Canada, 2019. Aluminum Facts [WWW Document]. URL https://www.nrcan.gc.ca/our-natural-resources/minerals-mining/minerals-metals-facts/aluminum-facts/20510#L2

Nova Pb inc., 2004. Présentation du procédés CalSiFrit [WWW Document]. URL http://142.44.245.8/sections/mandats/alcan-brasque/documents/DM1-1.pdf

Nunez, P., 2020. Sustainable Spent Pot Line Management Guidance. Miner. Met. Mater. Ser. 1225–1230. https://doi.org/10.1007/978-3-030-36408-3_168

Olivas, A., Ferraris, C.F., George, W.L., Garboczi, E.J., Toman, B., 2017. Certification of SRM 2493 : Standard Reference Mortar for Rheological Measurements, NIST Special Publication 260-187. https://doi.org/https://doi.org/10.6028/NIST.SP.260-187

Øye, H.A., 2017. Discussion of Industrial Spent Pot Lining Treatment, in: Proceedings of 35th International ICSOBA Conference. Hamburg, Germany, pp. 2–5.

Palomo, A., 2012. Alkaline Hydration of Tricalcium Aluminate 8, 1–8. https://doi.org/10.1111/j.1551-2916.2012.05348.x

Panesar, D.K., Francis, J., 2014. Influence of limestone and slag on the pore structure of cement paste based on mercury intrusion porosimetry and water vapour sorption measurements. Constr. Build. Mater. 52, 52–58. https://doi.org/10.1016/j.conbuildmat.2013.11.022

Personnet, P.B., 1999. Treatment and Reuse of Spent Pot Lining, an Industrial Application in a Cement Kiln, in: Essential Readings in Light Metals. John Wiley & Sons, Inc., Hoboken, NJ, USA, pp. 1049–1056. https://doi.org/10.1002/9781118647745.ch141

Poon, C.S., Lam, L., Wong, Y.L., 1999. Effects of Fly Ash and Silica Fume on Interfacial Porosity of Concrete. J. Mater. Civ. Eng. 11, 197–205. https://doi.org/10.1061/(ASCE)0899-1561(1999)11:3(197)

Roussel, N., 2012. Understanding the rheology of cement.

Scrivener, K., Martirena, F., Bishnoi, S., Maity, S., 2018. Cement and Concrete Research Calcined clay limestone cements (LC 3). Cem. Concr. Res. 114, 49–56. https://doi.org/10.1016/j.cemconres.2017.08.017

Scrivener, K., Snellings, R., Lothenbach, B., 2016. A Practical Guide to Microstructural Analysis of Cementitious Materials Edited, A Practical Guide to Microstructural Analysis of Cementitious Materials. https://doi.org/10.7693/wl20150205

Shanks, W., Dunant, C.F., Drewniok, M.P., Lupton, R.C., Serrenho, A., Allwood, J.M., 2019. How much cement can we do without ? Lessons from cement material fl ows in the UK 141, 441–454. https://doi.org/10.1016/j.resconrec.2018.11.002

Shi, C., Zheng, K., 2007. A review on the use of waste glasses in the production of cement and concrete 52, 234–247. https://doi.org/10.1016/j.resconrec.2007.01.013

Skibsted, J., Snellings, R., 2019. Reactivity of supplementary cementitious materials (SCMs) in cement blends. Cem. Concr. Res. 124, 105799. https://doi.org/10.1016/j.cemconres.2019.105799

Snellings, R., Chwast, J., Cizer, Ö., De Belie, N., Dhandapani, Y., Durdzinski, P., Elsen, J., Haufe, J., Hooton, D., Patapy, C., Santhanam, M., Scrivener, K., Snoeck, D., Steger, L., Tongbo, S., Vollpracht, A., Winnefeld, F., Lothenbach, B., 2018. Report of TC 238-SCM: hydration stoppage methods for phase assemblage studies of blended cements—results of a round robin test. Mater. Struct. Constr. 51. https://doi.org/10.1617/s11527-018-1237-5

Suraneni, P., Hajibabaee, A., Ramanathan, S., Wang, Y., Weiss, J., 2019. New insights from reactivity testing of supplementary cementitious materials. Cem. Concr. Compos. 103, 331–338. https://doi.org/10.1016/j.cemconcomp.2019.05.017

Suraneni, P., Weiss, J., 2017. Examining the pozzolanicity of supplementary cementitious materials using isothermal calorimetry and thermogravimetric analysis. Cem. Concr. Compos. 83, 273–278. https://doi.org/10.1016/j.cemconcomp.2017.07.009

Svermova, L., Sonebi, M., Bartos, P.J.M., 2003. Influence of mix proportions on rheology of cement grouts containing limestone powder. Cem. Concr. Compos. 25, 737–749.

https://doi.org/10.1016/S0958-9465(02)00115-4
Tavares, L.R.C., Junior, J.F.T., Costa, L.M., da Silva Bezerra, A.C., Cetlin, P.R., Aguilar, M.T.P., 2020. Influence of quartz powder and silica fume on the performance of Portland cement. Sci. Rep. 10, 21461. https://doi.org/10.1038/s41598-020-78567-w
Thiyagarajan, H., Mapa, M., Kushwaha, R., 2018. Investigation on the Rheological Behavior of Fly Ash Cement Composites at Paste and Concrete Level. J. Inst. Eng. Ser. A 99, 295–301. https://doi.org/10.1007/s40030-018-0284-9
Tironi, A., Trezza, M.A., Scian, A.N., Irassar, E.F., 2013. Assessment of pozzolanic activity of different calcined clays. Cem. Concr. Compos. 37, 319–327. https://doi.org/10.1016/j.cemconcomp.2013.01.002
Tokyay, M., 2016. Cement and Concrete Mineral Admixtures, CRC Press Taylor & Francis Group. CRC Press. https://doi.org/10.1201/b20093
Trümer, A., Ludwig, H.M., 2015. Sulphate and ASR resistance of concrete made with calcined clay blended cements. RILEM Bookseries 10, 3–9. https://doi.org/10.1007/978-94-017-9939-3_1
Vikan, H., Justnes, H., 2007. Rheology of cementitious paste with silica fume or limestone. Cem. Concr. Res. 37, 1512–1517. https://doi.org/10.1016/j.cemconres.2007.08.012
Wang, Y., Wang, D., Dong, C., Yang, Y., 2017. The behaviour and reactions of sodium containing minerals in ash melting process. J. Energy Inst. 90, 167–173. https://doi.org/10.1016/j.joei.2016.02.007
WBCSD, IEA, 2009. Cement Technology Roadmap 2009: Carbon emissions reductions up to 2050 36. https://doi.org/978-3-940388-47-6
Wesche, K., 1991. Fly Ash in Concrete : Properties and Performance, Report of Technical Committee 67-FAB Use of Fly Ash in Building RILEM. E & FN SPON.
Yu, Z., Ma, J., Ye, G., van Breugel, K., Shen, X., 2017. Effect of fly ash on the pore structure of cement paste under a curing period of 3 years. Constr. Build. Mater. 144, 493–501. https://doi.org/10.1016/j.conbuildmat.2017.03.182
Zhang, T., Gao, Peng, Gao, Pinhai, Wei, J., Yu, Q., 2013. Effectiveness of novel and traditional methods to incorporate industrial wastes in cementitious materials — An overview. "Resources, Conserv. Recycl. 74, 134–143. https://doi.org/10.1016/j.resconrec.2013.03.003